

## How Oxidised Grain Boundaries Fail

**Helen Dugdale, David E.J Armstrong, Ed Tarleton, Steve G. Roberts, Sergio Lozano-Perez \***

Department of Materials, University of Oxford, Parks Rd, OX1 3PH Oxford, UK

\* Corresponding author. Email: [sergio.lozano-perez@materials.ox.ac.uk](mailto:sergio.lozano-perez@materials.ox.ac.uk), Tel: +44 (0)1865273795

### **Abstract**

Macroscopic behaviour of materials is often controlled by microscopic events; this has driven interest in testing and analysing increasingly smaller features. The ability to perform mechanical tests on the micron-scale, with modelling and high resolution chemical and structural analysis on the same scale, now makes it possible to investigate in detail the mechanisms controlling one of the most complex modes of fracture: stress corrosion cracking (SCC). In this paper, through such a multifaceted approach, we show that individual grain boundaries, preferentially oxidized after exposure to simulated pressurized nuclear reactor cooling water, can be mechanically tested and their resistance to fracture quantified. These results have direct consequences in understanding the mechanisms controlling SCC propagation and initiation.

Keywords: Micro-/nanoindentation, Fracture stress, Grain boundary embrittlement, Tomography, Transmission electron microscopy (TEM)

### **1. Introduction**

Stress corrosion cracking (SCC) is one of the most challenging modes of materials failure. It is difficult to detect, monitor and predict and, therefore, it can only be avoided or delayed through a better understanding of its underlying mechanisms. In the nuclear industry, it affects many critical components. For example, SCC has degraded thousands of Alloy 600 tubes in heat exchangers, resulting in costly repairs. Alloy 600 is an austenitic alloy with a typical composition of 75wt% Ni, 15% Cr, 8wt% Fe, plus impurities of carbon, copper, manganese, nitrogen, sulphur and silicon. It was

originally chosen because of its high corrosion resistance and good high temperature properties. However, once in service, Alloy 600 was found to be prone to SCC, with the first observation being reported in 1959 [1,2,3].

Many mechanisms have been proposed in order to explain this degradation [4,5,6], none of which have been unambiguously experimentally verified. One of the most widely accepted is the mechanism of Selective Internal Oxidation (SIO) [7]. This relies on two relatively simple observations: that Alloy 600 is known to oxidise internally along grain boundaries in the presence of “primary” water [8] and that the failure of the alloy by SCC is intergranular. The proposed mechanism assumes that the Cr-rich oxide produced along the grain boundary is brittle, providing an easy crack pathway through the alloy. However, experimental evidence for this is very scarce [9], and until now it has not been possible to verify the failure mechanism and its relation to microstructure. In order to test the validity of the SIO mechanism, we have developed and used a novel technique to investigate the mechanical properties of individual grain boundaries.

Micro-mechanical bend experiments based on the testing of focused ion beam (FIB)-manufactured micro-scale cantilevers have shown to be capable of measuring elastic moduli [10,11], yield stress [9,12,13] and fracture toughness [14,15]. However these techniques have, to date, used model systems such as single crystals [14,15,16], and single phase materials [12]. In most advanced engineering materials, with complex polycrystalline microstructures, features at the microstructural level normally control behaviour; especially grain boundaries and precipitates. In order to understand better the link between microstructure and mechanical behaviour there is a need to combine micro-mechanical testing with microstructural observations at the same scale and on the same test element. This information can then be used to model fully the behaviour of the micro-cantilevers.

## **2. Experimental**

An Alloy 600 coupon that had been subjected to autoclave testing to produce grain boundary oxidation was provided by the Institute of Nuclear Safety Systems (INSS), Japan. The chemical composition was 0.017 C, 0.32 Mn, 8.57 Fe, 74.03 Ni and 16.21 Cr (all in wt.%). The coupon had been mill-annealed at 1050°C for 15 minutes after fabrication. The corrosion test was performed in an autoclave under simulated PWR primary water conditions (2.75 ppm  $\text{DH}_2$ , 500 ppm B and 2 ppm Li) at 360°C for 2700h. Test temperature was slightly higher than usual to accelerate oxidation.

Exposure to simulated PWR primary water resulted on the oxidation of the sample surfaces as well as the preferential oxidation of grain boundaries. Prior transmission electron microscopy (TEM) characterization had revealed that intergranular oxidation could reach depths over 5  $\mu\text{m}$  [17]. A Zeiss NVision 40 FIB-SEM was used for the preparation and imaging of the cantilevers. By examining the oxidized surface of the specimen, grain boundaries were selected that showed obvious signs of oxidation and which were perpendicular to the oxidized surface (checked by milling a small local trench). Cantilevers were prepared across them as described by Armstrong et al. [14]. Cantilevers were manufactured with a triangular cross-section ( $\approx 2\mu\text{m}$  wide) and 15 $\mu\text{m}$  long (see diagram in Figure 1).

After preparation, the cantilevers were tested in a MTS Nanoindenter XP, using a diamond Berkovich tip. The technique used for the micromechanical testing was a development of that described by Armstrong et al. [14]. The indenter tip was placed at the end of the cantilever and used to displace the cantilever at a constant rate of 5nm/s and a load-displacement curve recorded. In previous work, surface profilometry was performed using the NanoVision option in the MTS nanoindenter to image the cantilever prior to testing, allowing accurate placement of the tip on the end of the cantilever. In these experiments this was not possible. During scanning it was found that loosely bonded oxide particles on the top surface would be picked up on the end of the indenter tip and the scanning resolution was then insufficient to image the cantilever. Instead the indenter tip was aligned using series of microscope-to-indenter calibrations at high magnification, though the success rate of

testing was significantly lower than when using the scanning-imaging method. Once tested, the cantilevers were then imaged in a FIB-SEM (Zeiss NVision 40), where a FIB 3D slicing technique [18] was used to reconstruct the oxidized grain boundary portion of the cantilever in 3D. TEM characterization was performed in a Jeol 3000F equipped with a Gatan GIF and operated at 297keV. Electron energy-loss spectroscopy (EELS) analytical data were acquired in steps of 0.5nm. Convergence and collection half-angles of respectively 19 and 20mrad were used. A form of multivariate statistical analysis (MSA) consisting of a weighted principal component analysis combined with factor analysis [19,20] was used to identify the key sources of information in the dataset, allowing a "noise-free" dataset to be generated, from which all EELS data shown here were obtained.

### 3. Results

Sixteen cantilevers were prepared on the exposed surface of the Alloy 600 specimen that had been exposed to simulated PWR primary water. Figure 2a shows potentially oxidized grain boundaries, made obvious due to differences in the oxidation rate on the differently-oriented grains on either side. Cantilevers were prepared so that the grain boundary plane was close to the "fixed" end. Their mechanical response could be split into two categories: (a) cantilevers exhibiting plastic deformation but no fracture; and (b) cantilevers exhibiting brittle fracture along the grain boundary. Examples of each type are discussed in detail below:

*(a) Plastic Deformation and no fracture:* Five of the cantilevers tested (~31%) did not fracture, but simply exhibited plastic yield on the load/displacement curves, as shown in Figure 2 (green plot, plastic deformation). Figures 2b and 2c show typical examples of such cantilevers after testing; both cantilevers are shown after longitudinal cross-sectional surfaces have been exposed by FIB milling after testing. Slip lines are visible on the top surface in Figure 2b and it is clear that the cantilever has

deformed plastically. In figure 2c, slip lines can be seen on the side of the cantilever close to the grain boundary, though no fracture has occurred. The grain boundaries shown in figures 2b and 2c are only incompletely oxidised, even immediately near the exposed surface; this might have prevented crack initiation.

*(b) Brittle Fracture:* The majority of the cantilevers underwent some sort of fracture. Two main types of fracture behaviour were observed. Three cantilevers (~19%) exhibited complete fracture, unstably propagating through their full depth. A typical example is shown in Figure 2d where the crack has propagated along the fully oxidised grain boundary. Eight cantilevers (~50%) did not show full fracture, though some crack growth was found on examination after testing. In four cases (~25%), crack growth was small. Figure 2e shows a typical example in which a small crack was found close to the fixed end of the cantilever, together with evidence of plastic deformation in the cross-sectional view; such cantilevers are also bent down towards the bottom of the trench. In these cases, the load/displacement curve, Figure 3 (blue, stable fracture), shows no obvious fracture event. In the other four cases, such as the example in Figure 2f, the cantilever did fracture substantially, but the crack propagated only part-way through the cantilever – in this case, encountering a grain boundary precipitate. In these cases, a recognizable fracture event was found in the load/displacement curve; Figure 3 (red, unstable fracture).

The mechanical behaviour of even a single oxidized grain boundary was found to be inhomogeneous. The cantilevers shown in Figures 2c and 2f were produced on the same grain boundary, separated from each other by 2 $\mu$ m; one has fractured and one has not. In order to better understand these results, a more detailed characterization linking local microstructure and composition and fracture behaviour was required. FIB 3D slicing [18] and high-resolution analytical TEM [21] were used to characterize the tested regions.

Regions containing oxidized grain boundaries in the cantilevers were cross-sectioned and imaged in the FIB-SEM with nanometre resolution (see Figure 4). This sequential milling + imaging approach

(FIB 3D slicing) allowed 3D reconstructions of the crack path and intergranular oxidation (see Figure 5) with high detail (voxel size 10x10x30nm). It was found that:

1. As the SIO model suggests, fracture of grain boundaries is directly correlated with the presence of a grain boundary oxide film. In the cantilevers that had not fractured completely, the intergranular oxidation did not reach the lower part of the grain boundary, and fracture stopped where the oxide terminated.
2. However, contrary to the assumptions of the SIO model, when grain boundary fracture occurred, it never propagated through the oxide itself, but always along the oxide-metal interface. The fracturing interface was the one adjacent to the grain that exhibited an interface more nearly perpendicular to the stress direction (along the cantilever axis).
3. Crack paths could be modified significantly by the presence of grain boundary carbide particles (see Figure 2f). Grain boundary planes were found to have a ~50% carbide coverage. Intergranular carbides were elongated along the grain boundary plane (over 1µm in length), and were usually larger than the intragranular carbides (which were equiaxed with ~0.5µm diameter). These carbides, when in contact with the intergranular oxide, showed no signs of oxidation themselves but were surrounded by a Cr-depleted matrix that had preferentially oxidized (see Figure 4). This oxide surrounding the Cr-carbides was never observed to fracture during the tests.

In-situ lift out samples [22] containing the same oxidized grain boundary as that tested by micromechanics were prepared for TEM characterization. This allowed a comprehensive nano-scale analytical mapping including Energy Filtered TEM (EFTEM), Energy Dispersive X-ray (EDX) and EELS, as well as indexation of all the relevant crystallographic directions through electron diffraction and atomic resolution TEM. The surface oxide was found to have the structure previously found by Robertson et al. [23] consisting of an external Fe-rich spinel  $(\text{Fe, Ni})_3\text{O}_4$  and an internal Cr-rich oxide

(Cr, Fe)<sub>3</sub>O<sub>4</sub> (~30nm thick). In the oxidized grain boundaries, the position of these layers was reversed. The Cr-rich spinel had formed first, remaining at the centre of the oxidized portion. Then, when the locally-available Cr became depleted, Fe-rich spinel formed next to the oxide-metal interface (Figure 6). High-angle annular dark field (HAADF) imaging showed that the inner Fe-rich oxide (next to the metal) is often less dense than the outer Cr-rich oxide (see Figure 7). FIB 3D slicing revealed that fracture follows the interface between the oxide and the metal, which is exactly the area where this low-density Fe-rich oxide is observed (as arrowed in Figure 7).

In order to gain quantitative information about the strength of the weak oxide-metal interfaces produced at grain boundaries by SCC, finite element analysis (using Abaqus software) was carried out to model the fracture in the cantilever shown in Figures 2e and 2f. An image analysis algorithm was developed to extract the oxide and grain boundary geometry from the FIB 3D slicing model (Figure 5). This information was then used to generate a 3D finite element mesh of the beam with the same dimensions as in the experiment (Figure 8c). An isotropic elastic material law was used for the Alloy 600 beam with elastic constants  $E=270\text{GPa}$ ,  $\nu=0.3$  [24]. The carbide and associated oxide layer were modelled as a single elastic inclusion which was assumed to be stiffer than the matrix ( $E=500\text{GPa}$  and  $\nu=0.3$ ). A bi-linear cohesive law was used along the Alloy 600 grain boundary and oxide-Alloy 600 interface, with an initial stiffness  $K=1\text{GPa/nm}$  until a damage initiation stress  $\sigma_0$  is reached. The interface then softens until an opening displacement  $d_f$  at which point the interface fails. The cohesive parameters  $\sigma_0$ ,  $d_f$  were calibrated against the experimental load-displacement data; best fit values were  $\sigma_0 = 1.35\text{ GPa}$  and  $d_f = 5\text{ nm}$ . This corresponds to an interfacial fracture energy for the oxide-metal interfaces of  $G = 1/2 \sigma_0 d_f = 3.4\text{ J m}^{-2}$ . The predicted fracture behaviour using these parameters can be seen in the plot in Figure 3 (black line) and as a full fracture model in Figure 8.

#### 4. Discussion

The finite element modelling was able to accurately reproduce the “real” fracture events. Figure 8 shows that the observed fracture behaviour (Figure 8a) is comparable to that one predicted by the model (Figure 8b). The crack initiates where the oxidized grain boundary meets the free surface at the top of the beam and then propagates downwards, branching left around the oxide that surrounds the Cr carbide before arresting where the oxidized region finishes (Figure 2g). This creates a high stress region at the crack-tip which might cause the crack to continue to propagate along the un-oxidised grain boundary below the carbide. This did not occur in the experiment, indicating that the un-oxidised grain boundaries must be significantly stronger than oxidised boundaries. In order to reproduce this arrest behaviour in the model, the un-oxidised grain boundary interface required a minimum fracture energy of  $G = 25 \text{ J/m}^2$ .

After calculating the mechanical properties of oxidized grain boundaries and observing that the cracks tend to follow the oxide-metal interface, fracture along oxidized grain boundaries free of carbides was also simulated by finite element modelling. The overall stress to failure was found to be  $\approx 5\%$  higher in the boundaries with a carbide present (although the exact value depends strongly on the exact position and morphology of carbides). This suggests that grain boundary carbides can have a minor strengthening effect. The beneficial role of intergranular carbides in SCC of Alloy 600 under primary PWR conditions has been reported in the literature [25,26]. Various explanations have been given, including the formation of a denser and more protective Cr-rich oxide around the carbides [27] or their role as obstacles preventing grain boundary sliding [28]. This work suggests that a plausible explanation could be their role in deviating the crack from a straight path (grain boundary) into a more complex one following the oxide-metal interface around the carbide.

The finite element modelling indicated that a stress of 1.35GPa would be necessary to fracture the oxidized grain boundary tested in this work. It has been reported that minimum stresses of 350MPa are required to initiate SCC under PWR primary water conditions [29]. This initial discrepancy could have several explanations. Firstly, it should be noted that our fracture tests were performed in



vacuum and at room temperature, with no influence from the environment. If the environment plays an important role as a source of hydrogen, vacancies or other impurities, the measured values could be overestimating the minimum stress required to fracture. In addition, the relevant SCC mechanism involved in crack initiation could not be simply attributed to the formation of a brittle oxide phase, but also require the occurrence of additional factors (e.g. Hydrogen changing the mechanical properties locally [30]). Lastly, it should be noted that only one grain boundaries tested was fully characterized by TEM, FIB 3D and FEM; further analysis would be needed to produce statistically significant data and to get a view of the variability of fracture behaviour over a range of oxidised boundaries.

## **5. Conclusions**

Through the direct evidence found by micromechanical testing, FIB 3D slicing and TEM characterization, we can now understand how cracks propagate in oxidised grain boundaries, verifying (and modifying) the assumptions of the SIO model for grain-boundary stress corrosion cracking. A high-resolution characterization of the oxide-metal interface has shown the presence of a Fe-rich oxide, less dense than the original Cr-rich oxide; this is the weakest microstructural feature and it is used by the crack to propagate. Modelling of the behaviour of the test specimens has given, for the first time, quantitative information about grain boundary fracture strengths associated with this process. These results demonstrate how a multi-faceted approach, utilizing advanced characterisation techniques and modelling alongside micro-mechanical testing, can lead to a better understanding of the mechanical behaviour of grain boundaries. A remaining “grand challenge” problem is to model the properties of bulk materials in terms of these microstructural-scale behaviours.

## Acknowledgements

The authors are grateful to Dr Takuyo Yamada and Dr Takumi Terachi from INSS (Japan) for the provision and autoclave testing of the samples described in this manuscript. The Department of Materials (University of Oxford) is acknowledged for financial support.

## References

- [1] Coriou H. Industries Atomiques & Spatiales 1972;16:11.
- [2] Dutta RS. J.Nucl.Mater. 2009;393:343.
- [3] Andresen PL, Morra MM. Corrosion 2008;64:15.
- [4] Andresen PL, Ford FP. Mater. Sci. Eng. A-Struct. Mater. Prop. Microstruct. Process. 1988;A103:167.
- [5] Dewald D, Lee TC, Robertson IM, Birnbaum HK. Metallurgical-Transactions-A-(Physical-Metallurgy-and-Materials-Science) 1990;21A:2411.
- [6] Chateau JP, Delafosse D, Magnin T. Acta Materialia 2002;50:1523.
- [7] Scott, PM, Le Calvar, M. Proceedings of the Sixth International Symposium on Environmental Degradation of Materials in Nuclear Power Systems - Water Reactors 1993:657.
- [8] Combrade, P, Scott, PM, Foucault, M, Andrieu, E, Marcus, P. Proceedings of the Twelfth International Conference on Environmental Degradation of Materials in Nuclear Power Systems-Water Reactors 2005:883.
- [9] Fujii K, Fukuya K. Materials Transactions 2011;52:20.
- [10] Gong J, Wilkinson A. Philosophical Magazine Letters 2010;90:503.
- [11] Armstrong DEJ, Wilkinson AJ, Roberts SG. J.Mater.Res. 2009;24:3268.
- [12] Gong J, Wilkinson AJ. Acta Materialia 2009;57:5693.
- [13] Motz C, Schöberl T, Pippan R. Acta Materialia 2005;53:4269.
- [14] Armstrong DEJ, Wilkinson AJ, Roberts SG. Philosophical Magazine Letters 2011;91:394.
- [15] Di Maio D, Roberts SG. J.Mater.Res. 2005;20:299.
- [16] Wurster S, Motz C, Pippan R. Philosophical Magazine 2012;92:1803.
- [17] Terachi, T, Yamada, T, Arioka, K, Lozano Perez, S. Proceedings of the International Symposium on Research for Ageing Management of Light Water Reactors 2007:215.
- [18] Lozano-Perez S, Kruska K, Iyengar I, Terachi T, Yamada T. Corros.Sci. 2012;56:78.

- [19] Trebbia P, Bonnet N. Ultramicroscopy 1990;34:165.
- [20] Lozano-Perez S, de Castro Bernal V, Nicholls RJ. Ultramicroscopy 2009;109:1217.
- [21] Lozano-Perez S, Yamada T, Terachi T, Schröder M, English CA, Smith GDW et al. Acta Materialia 2009;57:5361.
- [22] Giannuzzi, LA, Drown, JL, Brown, SR, Irwin, RB, Stevie, FA. Materials Research Society Symposium - Proceedings 1997;480:19.
- [23] Robertson J. Corros.Sci. 1991;32:443.
- [24] Kumar A, Rabe U, Hirsekorn S, Arnold W. Appl.Phys.Lett. 2008;92
- [25] Was GS, Sung JK, Angelu TM. Met Trans A (Phys Met and Mat Sci) 1992;23A:3343.
- [26] Scarberry RC, Pearman SC, Crum JR. Corrosion 1976;32, no.10:401.
- [27] Thomas LE, Bruemmer SM. Corrosion 2000;56, no.6:572.
- [28] Arioka K, Yamada T, Terachi T, Chiba G. Corrosion 2006;62:568.
- [29] Itoh, H, Kutomi, Y, Mukai, M, Sakai, K. Proceedings of ICONE5 1997:403.
- [30] Birnbaum HK, Sofronis P. Materials Science and Engineering A 1994;176:191.

## Figures

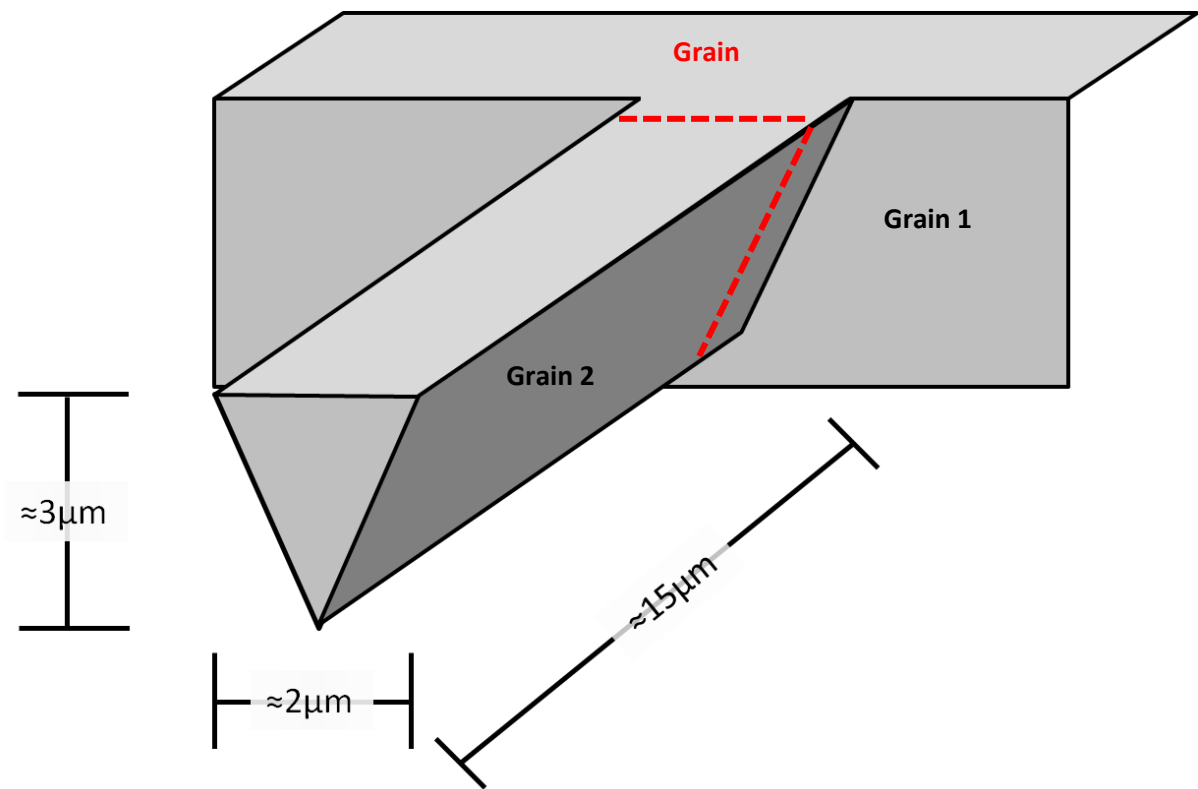


Figure 1: Schematic of triangular micro-cantilever

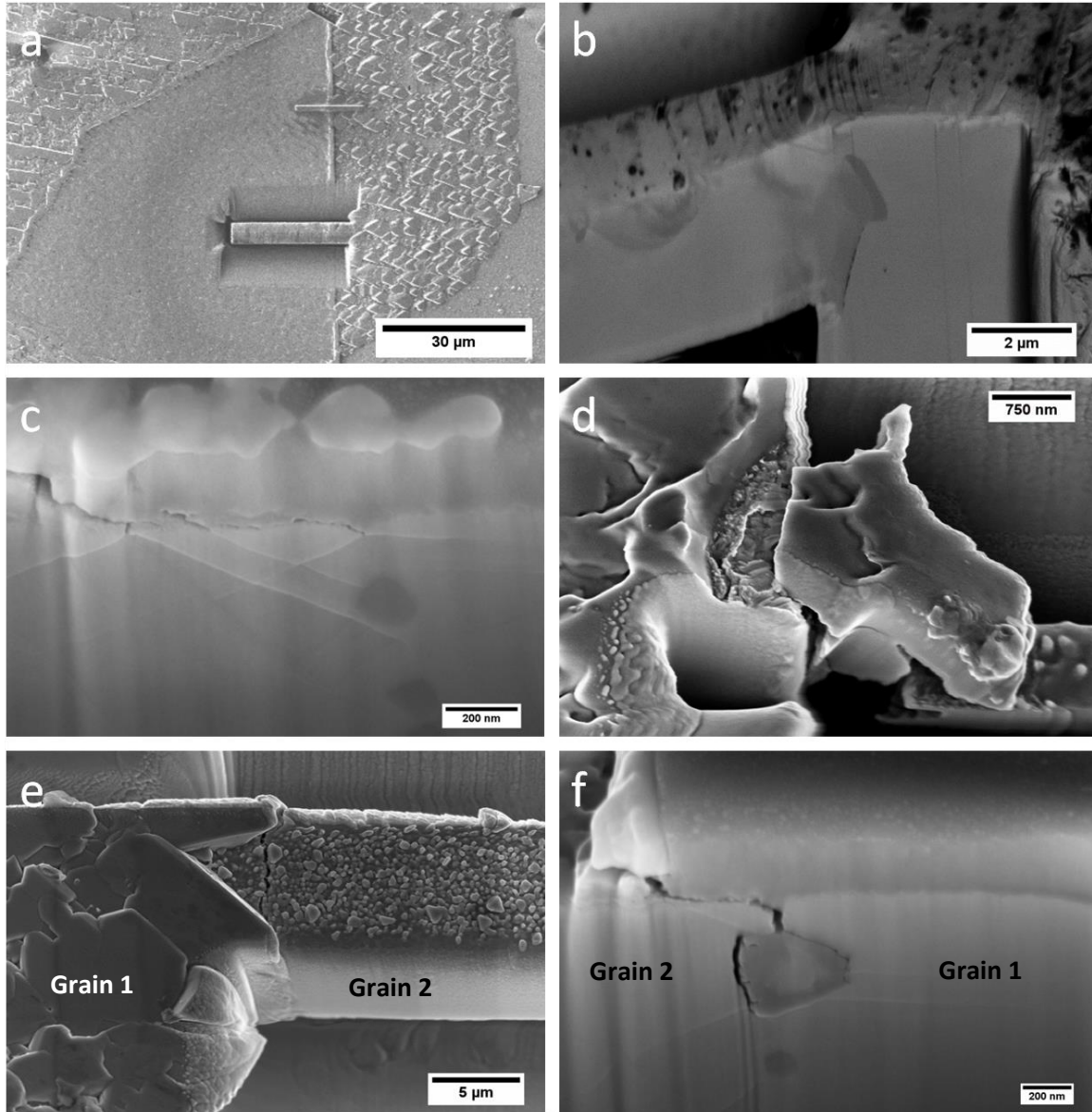


Figure 2: FIB SE images showing: (a) untested microcantilever and three observed deformation modes: (b) (c) plastic deformation without fracture, (d) intergranular brittle fracture and (e)-(f) intergranular crack growth without total fracture.

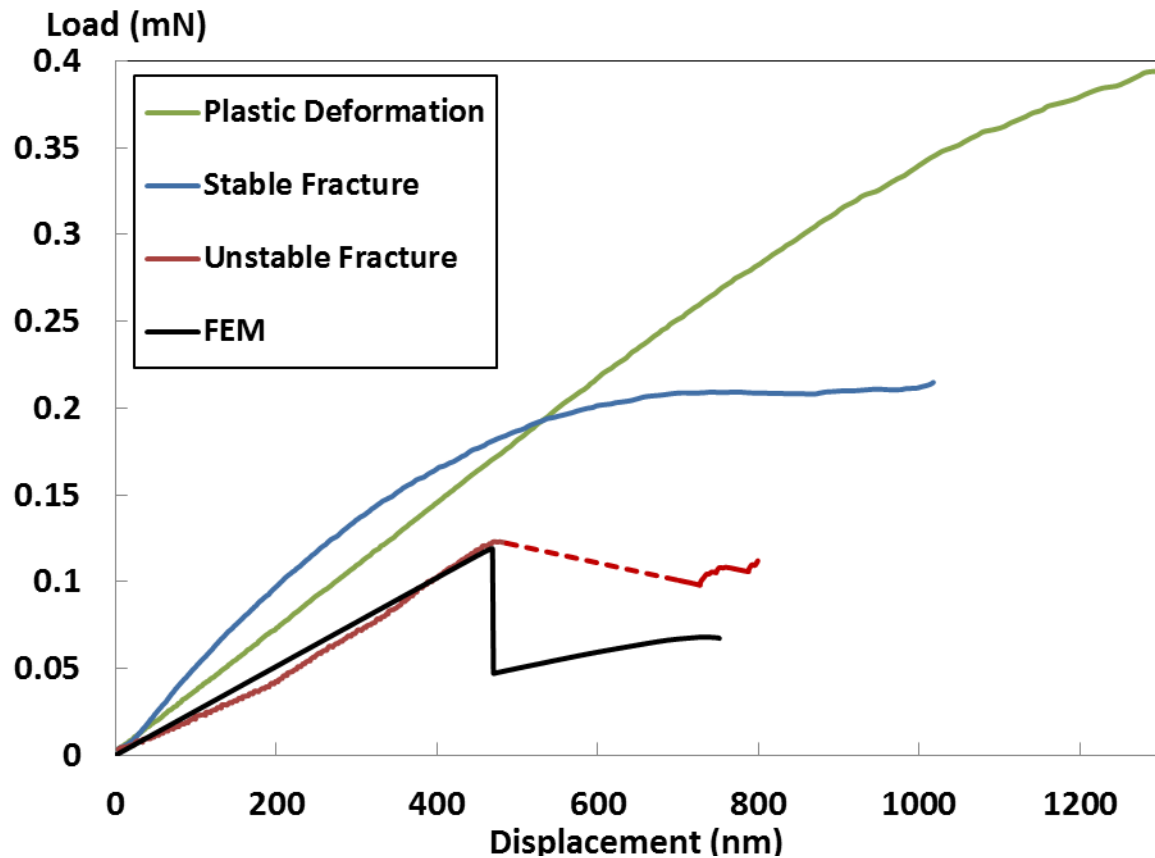


Figure 3: Typical load-displacement curves for three cantilevers, showing plastic, stable fracture and unstable fracture events.

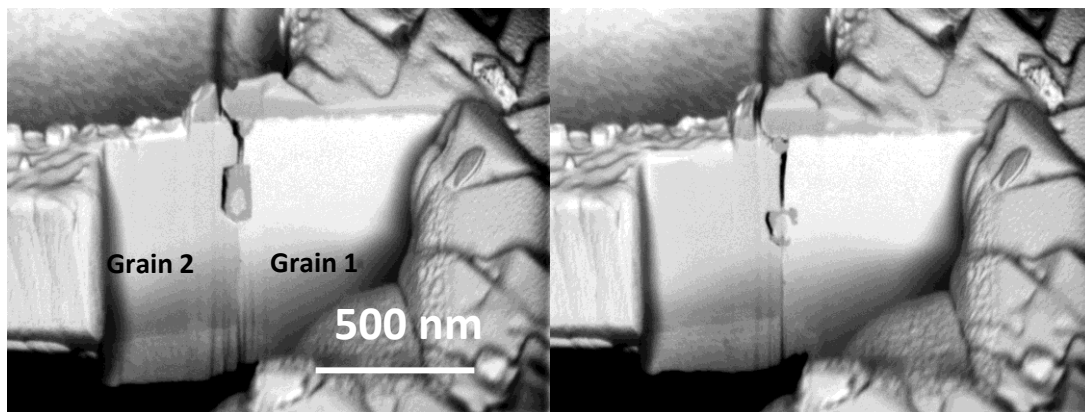


Figure 4: FIB SE images showing a cross-sectional view of the base of cantilever after testing. Original surface oxide, crack path (black), internal oxides (dark grey) and an intergranular carbide (light grey) are clearly visible. Left and right images show the crack path at different sections during the FIB 3D slicing acquisition.

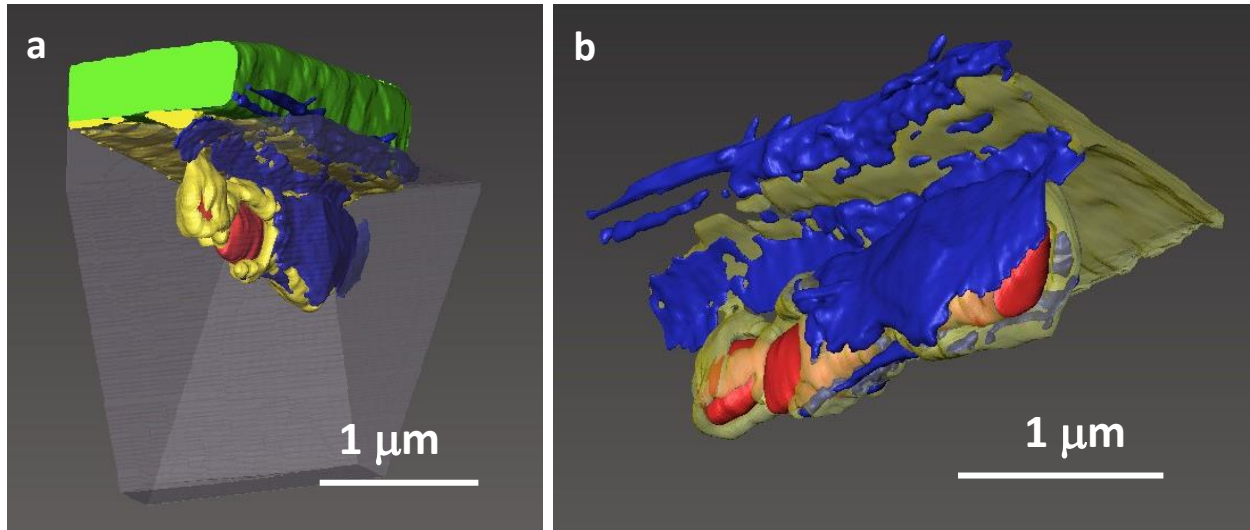
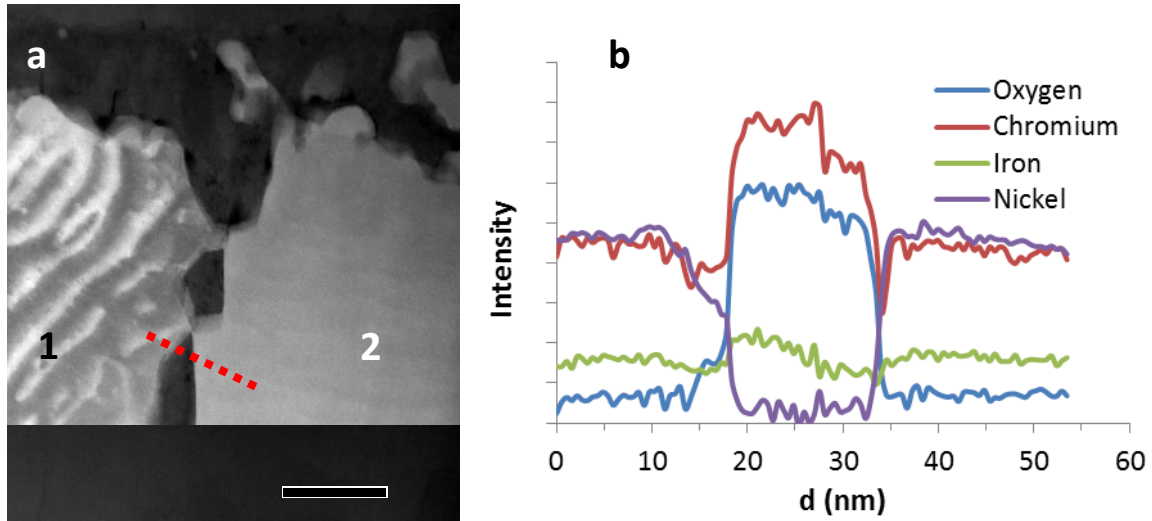


Figure 5: 3D models generated from the FIB 3D sequential sectioning showing the various items reconstructed: carbides (red), Fe-rich external oxide (green), Cr-rich internal oxide (yellow) and open crack (dark blue). (a) shows all the features together with a portion of the cantilever (semi-transparent). (b) shows the crack path in detail and how it follows the oxide-metal interface, although the crack depth is not homogeneous along the boundary.



Figures 6: (a) STEM ADF image showing a cross-sectional view of the oxidized grain boundary next to exposed surface. Grains are labelled as 1 and 2. (b) EELS line-scan across the oxidized boundary. Spectra acquired in steps of 0.5nm. Every mark in the y-axis is equal to 20000 electrons. A Cr-depleted (and therefore Fe-rich) oxide can be observed at each of the oxide-metal interfaces. A 5% relative error is assumed for the plots in (b).



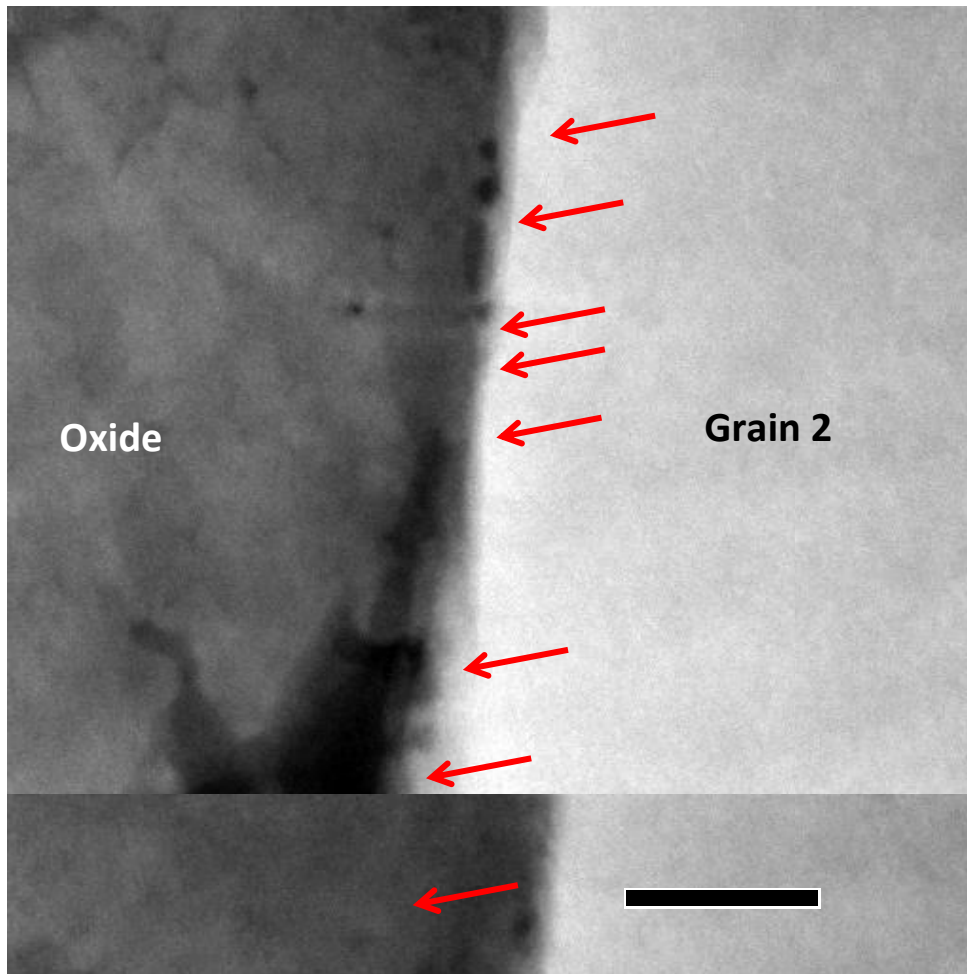


Figure 7: HAADF image showing the oxide-metal in grain 2. The darker regions (arrowed) at the oxide near the interface can be interpreted as having a lower density than the oxide further away.

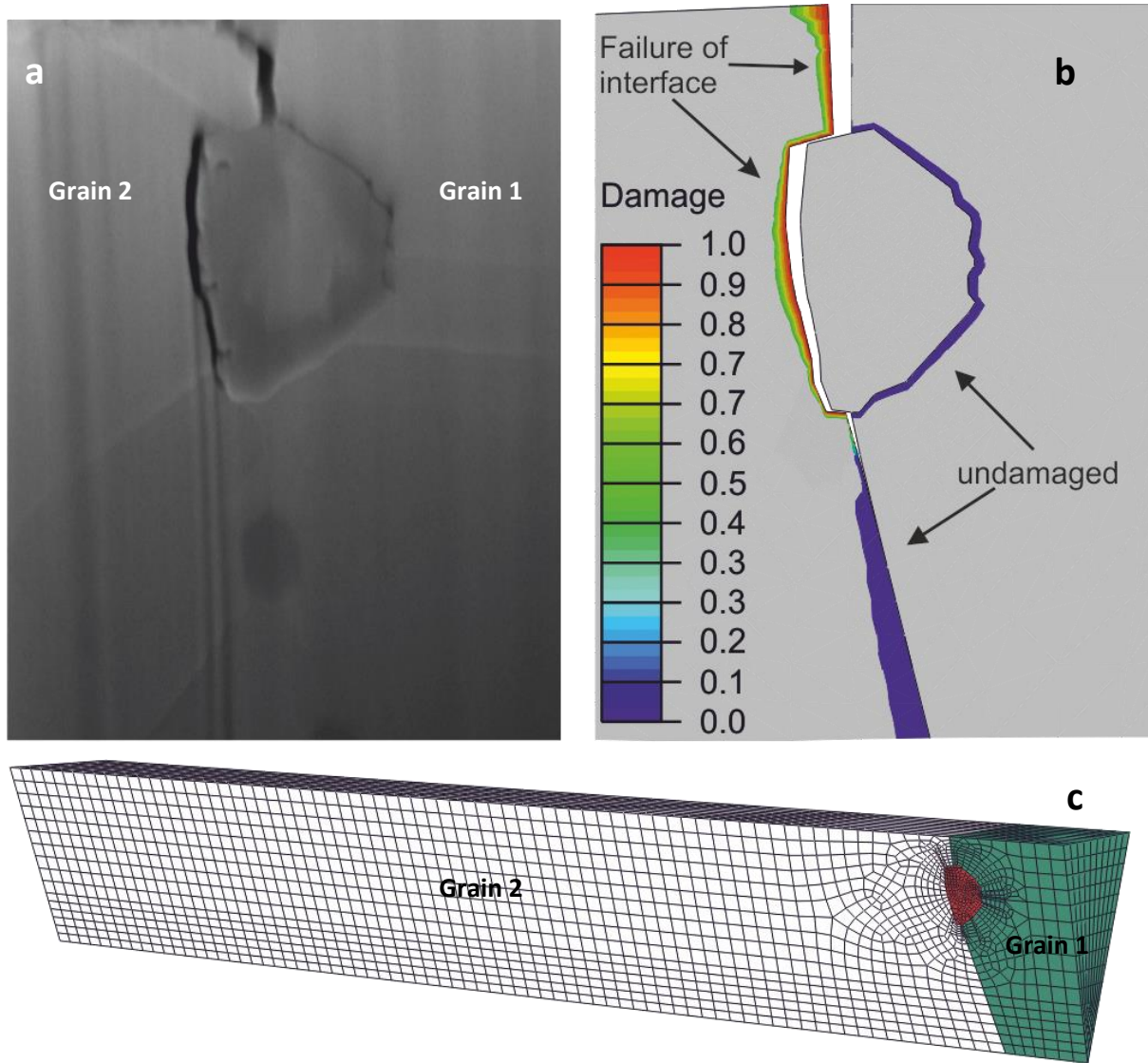


Figure 8: SEM SE cross-sectional view of cantilever after testing, where it can be seen that the crack has propagated along the oxidized grain boundary and then along the oxide-metal interface around the oxide surrounding the carbide (a) and the predicted damage obtained from the finite element model (b). The mesh (extracted from FIB 3D slicing reconstruction) is shown before testing (c).